

FAMES: Fast Approximate Multiplier Substitution for Mixed-Precision Quantized DNNs—Down to 2 Bits!

Yi Ren¹, Ruge Xu¹, Xinfei Guo¹, and Weikang Qian¹

¹ University of Michigan – Shanghai Jiao Tong University Joint Institute, Shanghai Jiao Tong University, Shanghai, China
E-mail: {201705-renyi, schrodinger, xinfei.guo, qianwk}@sjtu.edu.cn

Abstract—A widely-used technique in designing energy-efficient deep neural network (DNN) accelerators is quantization. Recent progress in this direction has reduced the bitwidths used in DNN down to 2. Meanwhile, many prior works apply approximate multipliers (AppMuls) in designing DNN accelerators to lower their energy consumption. Unfortunately, these works still assume a bitwidth much larger than 2, which falls far behind the state-of-the-art in quantization area and even challenges the meaningfulness of applying AppMuls in DNN accelerators, since a high-bitwidth AppMul consumes much more energy than a low-bitwidth exact multiplier! Thus, an important problem to study is: Can approximate multipliers be effectively applied to quantized DNN models with very low bitwidths? In this work, we give an affirmative answer to this question and present a systematic solution that achieves the answer: FAMES, a fast approximate multiplier substitution method for mixed-precision DNNs. Our experiments demonstrate an average 28.67% energy reduction on state-of-the-art mixed-precision quantized models with bitwidths as low as 2 bits and accuracy losses kept under 1%. Additionally, our approach is up to 300× faster than previous genetic algorithm-based methods.

Index Terms—Edge AI, Approximate Computing, Mixed-Precision Quantization

I. INTRODUCTION

In recent years, *artificial intelligence* (AI) has garnered significant attention due to its ability to provide real-time responses, reliability, and enhanced privacy. Among various AI models, *deep neural networks* (DNNs) stand out for their excellent performance in applications like natural language processing [1], [2] and computer vision [3], [4]. However, as DNN models increase in size and complexity, their energy consumption rises significantly, which poses challenges for their deployment in environments with limited energy source [5].

Therefore, various methods have been proposed to improve the energy efficiency of the models. Among these methods, two notable ones are *quantization* [6], [7] and using *approximate multipliers* (AppMuls) [8], [9]. Quantization works by transforming values from high precision, such as 32-bit floating-point values, into lower precision representations like 8-bit fixed-point values [10]. It can not only reduce the memory footprint required for model storage, but also lower the energy consumption by using low-bitwidth arithmetic circuits. On the other hand, using AppMuls (hereafter referred to as *approximation* for short) involves substituting exact multipliers with AppMuls. Those AppMuls can reduce circuit area, delay, and energy consumption by sacrificing some accuracy in the computation result, which can be well tolerated by DNN applications.

However, there is a significant disparity between the bitwidths utilized in quantization studies and those in approximation studies, as illustrated in Table I. Quantization techniques have successfully reduced the bitwidths to the range of 2–5 bits [11], [12], [7]. In contrast, most research on approximation still uses 8×8 AppMuls [8],

TABLE I
SUMMARY OF RELATED WORK.

Work	Technique	Bit-Width		Multiplier
		Weight	Activation	
[13]	Approximation	4/5/6/8	8	Approximate
AdaPT [14]	Approximation	8	8	Approximate
[15]	Approximation	6/7/8	8	Approximate
ALWANN [8]	Approximation	8	8	Mixed ²
MARLIN [9]	Approximation	8	8	Mixed ²
PACT [12]	Quantization	2/3/4/5	2/3/4/5/32	Accurate
LQ-Nets [16]	Quantization	2/3/4	2/3/4/32	Accurate
HAWQ-V3 [7]	Quantization	4/8 MP ¹	4/8 MP ¹	Accurate
Ours	Approximation	2-8 MP ¹	2-8 MP ¹	Mixed ²

¹ Mixed precision.

² Mixed AppMuls.

[9], which falls far behind the state-of-the-art in the quantization area. Even worse, this challenges the meaningfulness of applying AppMuls in DNN accelerators, since a high-bitwidth AppMul consumes much more energy than a low-bitwidth exact multiplier and also diminishes the important benefit of low memory footprint brought by the low-bitwidth quantization. Thus, an important problem to study is: Can approximate multipliers be effectively applied to quantized DNN models with very low bitwidths?

Besides the above unsolved problem, another challenge faced by approximation is the excessive runtime to apply this technique, which comes from two sources: the algorithm to select different AppMuls for different layers in DNN and the fine-tuning process. While quantization is limited to a small number of bitwidths, approximation may search from hundreds of AppMul designs, resulting in a significantly larger search space. Therefore, traditional methods used in quantization, such as the NSGA algorithm [17], are less efficient in the case of approximation [8], [9]. On the other hand, the software simulation of AppMuls in the DNN model is usually slower than direct multiplication, making the retraining process of approximation, which is sometimes necessary to recovery the accuracy loss, much slower than quantization. These runtime issues are a bottleneck for approximation.

To address the above challenges, this work presents FAMES, a fast approximate multiplier substitution method for mixed-precision DNNs without retraining. Using FAMES, we successfully apply AppMuls to quantized DNN models with bitwidths as low as 2 bits, and the accuracy loss is less than 1%. Furthermore, FAMES shows a significant speed-up in selecting AppMuls, being 300× faster than the existing genetic algorithm (GA)-based selection methods. The key contributions of this work include:

- 1) We propose a new method to model the error of an AppMul through a novel *counting matrix*, which serves as a backbone of FAMES (see Section IV-B).

- 2) We introduce a Taylor expansion-based technique to efficiently estimate the loss perturbation of an AppMul on a DNN model based on the above error modeling (see Section IV-C). Its core components only need be computed once, making the algorithm efficient, even when evaluating numerous AppMuls.
- 3) We propose an integer linear programming (ILP)-based method for selecting the optimal AppMul for each layer, leverages the above estimation of loss perturbation as the minimization target (see Section IV-D).
- 4) We present results of applying AppMuls in conjunction with the state-of-the-art quantization techniques, extending the use of AppMuls to 2-bit precision. On average, our method achieves a 28.67% energy reduction over the corresponding quantized model **of the same bitwidth** with less than 1% accuracy loss.
- 5) We also make the code of FAMES open-source at XXX (the code is on GitHub and will be public after acceptance).

II. RELATED WORKS

A. Quantization

The prior quantization works fall into two categories, using uniform quantization and using mixed quantization. Works on uniform quantization often restore the accuracy through learnable quantizers. For instance, LQ-Nets [16] learns quantizers of weights and activations, and PACT [12] learns the clipping parameter of activations. These works usually perform well at 3-bit precision, but suffer from significant accuracy drop at 2 bits. This challenge actually offers an opportunity to approximation: If we can apply AppMuls in low-bitwidth DNN models without much accuracy drop, then it is possible to further reduce energy consumption without necessitating additional precision reduction. Works on mixed-precision quantization assign different bitwidths for each layer by measuring the impact of each layer on the model, which is called *layer sensitivity*. For instance, HAWQ-V3 [7] measures layer sensitivity by the Hessian matrix of the model's loss *w.r.t.* the weight tensor of each layer. These works usually adapt a wide range of bitwidths for each layer, from 2×2 to 8×8 , creating opportunities for the application of AppMuls on those layers with high bitwidths since approximating high-bitwidth multipliers typically introduces minimal error while significantly reducing the energy consumption [18], [13]. In conclusion, if achievable, AppMuls would improve the performance of both types of quantizations.

B. Approximate Multiplier

The prior works on AppMuls fall into three categories. The first category proposes new libraries of AppMuls [18], [13]. It typically focuses on introducing high-quality AppMuls by efficient design space exploration [18]. The second category develops efficient frameworks to speed up the training and inference process of DNNs with AppMuls [14], [15]. These two categories of works mainly work on $8 \times N$ AppMuls and apply the same AppMuls across all layers, which makes their results less energy-efficient than quantization works with lower bitwidth [11], [7]. The third category of works aims to find the optimal selection of AppMuls for each layer. For instance, ALWANN [8] and MARLIN [9] tackle the optimization problem using the NSGA-II algorithm [17]. However, these GA-based methods involve numerous iterations to achieve optimal results, making them impractical for large datasets like ImageNet.

III. PRELIMINARY

A. Notations

In the rest of the paper, we will use the terms *matrix* and *tensor* interchangeably, and we will use the following notations unless

otherwise specified. We use lowercase letters (*e.g.*, x) and uppercase letters (*e.g.*, Y) to denote vectors and matrices, respectively. We denote the index of an element in a vector/matrix in subscript. For instance, x_k denotes the k -th element of a vector x , and $Y_{i,j}$ denotes the element at row i and column j of a matrix Y . When we apply AppMuls on layers, the layer index k and the AppMul AM_k used for that layer are indicated inside a pair of parentheses in superscript. For instance, $Y^{(k,AM_k)}$ indicates the layer output of the k -th layer substituted with AppMul AM_k for all the multiplication operations in the layer. For simplicity, we drop AM_k from the superscript if an exact multiplier is applied. For instance, $Y^{(k)}$ represents the output of the k -th layer when an exact multiplier is used.

In practice, the input, the weight, and the output tensors in DNN models have four dimensions. For simplicity, we ignore the first two. Also, we use a lowercase letter to denote a vector flattened from the matrix referred to by the corresponding uppercase letter. For instance, X and x represent a matrix and a vector flattened from the matrix, respectively. Assuming that X is an $N \times N$ matrix, the *flattened vector* x satisfies that $x_{iN+j} = X_{i,j}$.

B. Quantization

Uniform quantization maps floating-point values to fixed-point values that are uniformly distributed. Given an input matrix V , the transformation between the floating-point element $V_{i,j}$ and the corresponding quantized element $\hat{V}_{i,j}$ is as follows:

$$\hat{V}_{i,j} = \text{round}\left(\frac{V_{i,j} - b}{s}\right), \quad (1)$$

$$V_{i,j} \approx s\hat{V}_{i,j} + b, \quad (2)$$

where s is the scaling factor and b is the offset. In DNN models, the convolution operation between the input matrix and the weight matrix is typically implemented using the sum of element-wise multiplication. Given the input matrix $X^{(k)}$ and the weight matrix $W^{(k)}$, the entry $Y_{i,j}^{(k)}$ ($1 \leq i \leq R, 1 \leq j \leq C$) of the output matrix Y is calculated as:

$$Y_{i,j}^{(k)} = \sum_{m=1}^R \sum_{n=1}^C X_{i+m,j+n}^{(k)} W_{m,n}^{(k)}, \quad (3)$$

where R and C are the kernel width and kernel height, respectively. By applying Eq. (2) to Eq. (3), we can derive the quantized version of the convolution operation as shown below:

$$Y_{i,j}^{(k)} = \sum_{m=1}^R \sum_{n=1}^C (s_X s_W \hat{X}_{i+m,j+n}^{(k)} \hat{W}_{m,n}^{(k)} + s_X b_W \hat{X}_{i+m,j+n}^{(k)} + s_W b_X \hat{W}_{m,n}^{(k)} + b_X b_W), \quad (4)$$

where s_X and b_X are the scaling factor and the offset, respectively, for quantizing the input matrix $X^{(k)}$, and s_W and b_W are the scaling factor and the offset, respectively, for quantizing the weight matrix $W^{(k)}$. By this transformation, the floating-point multiplication of $X_{a,b}^{(k)}$ and $W_{c,d}^{(k)}$ can be calculated using the fixed-point multiplication of $\hat{X}_{a,b}^{(k)}$ and $\hat{W}_{c,d}^{(k)}$.

C. Approximation

During approximation, an exact fixed-point multiplier is replaced by an approximate fixed-point multiplier. To model the behavior of the AppMul, a look-up table (LUT) is used here to store the input-output relation of the AppMul. Specifically, for an $N \times N$ AppMul AM_k , a $2^N \times 2^N$ matrix $M^{(k,AM_k)}$ is formed, where $M_{i,j}^{(k,AM_k)}$ ($0 \leq i \leq 2^N - 1, 0 \leq j \leq 2^N - 1$) stores the output of the AppMul AM_k when the two inputs are i and j . By substituting the quantized exact

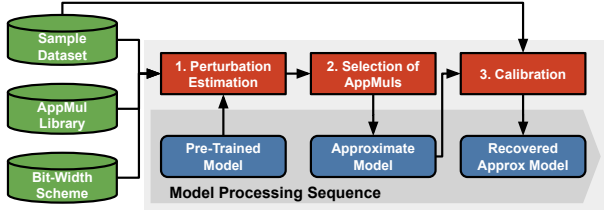


Fig. 1. Workflow of FAMES.

multiplication with the approximate one in Eq. (4), we can obtain the following equation:

$$Y_{i,j}^{(k,AM_k)} = \sum_{m=1}^R \sum_{n=1}^C (s_X s_W M_{\hat{X}_{i+m,j+n}^{(k)}, \hat{W}_{m,n}^{(k)}}^{(k,AM_k)} + s_X b_W \hat{X}_{i+m,j+n}^{(k)} + s_W b_X \hat{W}_{m,n}^{(k)} + b_X b_W). \quad (5)$$

D. Learnable Weight Clipping

In FAMES, we apply the Learnable Weight Clipping (LWC) quantizer in OmniQuant [19] to help recover accuracy. We introduce this method in this section. Its core concept is to use learnable upper and lower bounds to calibrate the weight matrix for each layer, which are dynamically updated through gradient descent during back-propagation in the calibration process. The calibrated weight matrix W' is calculated as follows:

$$W' = \text{clip}(W, \sigma(\gamma) \min(W), \sigma(\beta) \max(W)), \quad (6)$$

where W is the weight matrix, γ and β are the learnable lower and upper bounds, σ is the sigmoid function, and $\text{clip}(x, \min, \max)$ returns x , \min , and \max for x in $[\min, \max]$, $(-\infty, \min)$, and (\max, ∞) , respectively. During back-propagation, the gradient of loss L w.r.t. γ or β is calculated by applying the chain rule, e.g., $\frac{\partial L}{\partial \beta} = \frac{\partial L}{\partial W'} \frac{\partial W'}{\partial \beta}$, where $\frac{\partial L}{\partial W'}$ is calculated by back-propagation and the gradient of the calibrated weight matrix W' w.r.t. γ or β is calculated as follows:

$$\frac{\partial W'}{\partial \gamma} = \begin{cases} 0, & W \in (\min(W'), +\infty) \\ \min(W')(1 - \sigma(\gamma)), & W \in (-\infty, \min(W')] \end{cases},$$

$$\frac{\partial W'}{\partial \beta} = \begin{cases} 0, & W \in (-\infty, \max(W')) \\ \max(W')(1 - \sigma(\beta)), & W \in [\max(W'), +\infty) \end{cases}.$$

IV. PROPOSED METHOD

A. Overview

Our goal is to generate a high-accuracy energy-efficient NN model using AppMuls (hereafter referred to as *approximate model* for simplicity) from the pre-trained quantized NN model, where every multiplication within a convolutional layer is substituted by a specific type of AppMul assigned to that layer. To achieve it, we apply a three-step procedure as shown in Fig. 1. The inputs to our method include the pre-trained model, the bitwidth setting of each layer, a batch of samples from the target dataset, and the AppMul library. In the first step, we estimate the perturbation to the model's loss caused by applying the AppMuls using the batch of samples, which serves as a measure of the impact of the AppMuls. To facilitate the estimation, we introduce an error modeling of an AppMul through a novel counting matrix in Section IV-B. Based on the error modeling, we show the details of the perturbation estimation in Section IV-C. In the second step, the choice of the optimal AppMul for each layer to reduce the energy consumption is formulated as an ILP problem based on the perturbation estimation and then solved. The details will be described in Section IV-D. In the third step, the approximate model is calibrated to recover the accuracy, which will be described in Section IV-E.

B. Error Modeling of AppMul by Counting Matrix

If we subtract Eq. (4) from Eq. (5), we get the following equation:

$$Y_{i,j}^{(k,AM_k)} = Y_{i,j}^{(k)} + s_X s_W \sum_{m=1}^R \sum_{n=1}^C E_{\hat{X}_{i+m,j+n}^{(k)}, \hat{W}_{m,n}^{(k)}}^{(k,AM_k)}, \quad (7)$$

where $E_{\hat{X}, \hat{W}}^{(k,AM_k)} = M_{\hat{X}, \hat{W}}^{(k,AM_k)} - \hat{X}\hat{W}$ is an element of the error matrix $E^{(k,AM_k)}$ that stores the difference of the multiplication results between the AppMul AM_k and the exact multiplier. To show the impact of the error matrix $E^{(k,AM_k)}$ more directly, we transform the second term of Eq. (7) into the convolution of a *counting matrix* $C^{(k,i,j)}$ with the error matrix $E^{(k,AM_k)}$, where $C^{(k,i,j)}$ is a matrix related to the output $Y_{i,j}^{(k)}$ that tracks the number of occurrences of each possible multiplication input pairs during the calculation of $Y_{i,j}^{(k)}$. Specifically, the element at row a and column b in $C^{(k,i,j)}$, i.e., $C_{a,b}^{(k,i,j)}$, records the number of occurrences of the quantized multiplication on inputs a and b during the calculation of $Y_{i,j}^{(k)}$. For instance, if the quantized values 4 and 5 are multiplied 6 times in the calculation of $Y_{2,3}^{(1)}$, then $C_{4,5}^{(1,2,3)} = 6$. It should be noted that the value of $C^{(k,i,j)}$ is only relevant to the quantized inputs $\hat{X}^{(k)}$ and $\hat{W}^{(k)}$ and irrelevant to the error matrix of the approximate multiplier AM_k . By the definition of the counting matrix, it can be shown that Eq. (7) can be transformed to the following one:

$$Y_{i,j}^{(k,AM_k)} = Y_{i,j}^{(k)} + s_X s_W \sum_{m=0}^{2^N-1} \sum_{n=0}^{2^N-1} C_{m,n}^{(k,i,j)} E_{m,n}^{(k,AM_k)} \quad (8)$$

$$= Y_{i,j}^{(k)} + s_X s_W (c^{(k,i,j)})^T e^{(k,AM_k)}.$$

C. Perturbation Estimation

This section shows how we calculate the loss perturbation caused by the error introduced by applying an AppMul to a certain layer, which will be used later in our ILP formulation to facilitate the selection of the optimal AppMuls. As Eq. (8) shows, the flattened error vector $e^{(k,AM_k)}$ of AppMul AM_k for the k -th layer is an input of the layer output and hence, an input of the approximate model. Given that, we apply the Taylor expansion to estimate the loss perturbation $\Omega^{(k,AM_k)}$ caused by using the AppMul AM_k on the k -th layer as follows:

$$\Omega^{(k,AM_k)} = L^{(k,AM_k)} - L^{(k)} = L(Y^{(k,AM_k)}) - L(Y^{(k)})$$

$$= L(e^{(k,AM_k)}) - L(e^{(k,exact)}) \quad (9)$$

$$\approx g_{e^{(k)}}^T e^{(k,AM_k)} + \frac{1}{2} (e^{(k,AM_k)})^T H_{e^{(k)}} e^{(k,AM_k)},$$

where $g_{e^{(k)}} = \nabla L(e^{(k)})$ is the first-order gradient of L w.r.t. the error vector $e^{(k)}$, and $H_{e^{(k)}} = \nabla^2 L(e^{(k)})$ is the second-order Hessian matrix of L w.r.t. the error vector $e^{(k)}$. Since $e^{(k,exact)}$ represents the error matrix of the exact multiplier, which is a zero matrix, thus the difference in error matrix is simply the error matrix of the AppMul AM_k . We will show how the gradient $g_{e^{(k)}}$ and the Hessian $H_{e^{(k)}}$ of the error matrix are derived in Sections IV-C1 and IV-C2, respectively. As we will reveal, $g_{e^{(k)}}$ and $H_{e^{(k)}}$ are derived from the model parameters and the input distribution, which are irrelevant to the choice of AppMuls. Therefore, they only need to be calculated once, which makes the estimation method efficient even for estimating many AppMuls.

1) *Gradient*: The gradient of loss w.r.t. the error vector $e^{(k)}$ is a vector with the gradient of loss w.r.t. each element $e_m^{(k)}$ ($0 \leq m \leq 2^{2N} - 1$) calculated as follows:

$$\begin{aligned}
\frac{\partial L}{\partial e_m^{(k)}} &= \sum_{i=1}^N \sum_{j=1}^N \frac{\partial L}{\partial Y_{i,j}^{(k)}} \frac{\partial Y_{i,j}^{(k)}}{\partial e_m^{(k)}} \quad (\text{by chain rule}) \\
&= \sum_{i=1}^N \sum_{j=1}^N \frac{\partial L}{\partial Y_{i,j}^{(k)}} s_{ASW} c_m^{(k,i,j)} \quad (\text{by replacing } Y_{i,j}^{(k)} \text{ by Eq. (8)}).
\end{aligned} \tag{10}$$

where $\frac{\partial L}{\partial Y_{i,j}^{(k)}}$ is the gradient of loss w.r.t. $Y_{i,j}^{(k)}$, which is calculated by back-propagation, $c_m^{(k,i,j)}$ is the m -th element of the counting vector $c^{(k,i,j)}$ flattened from $C^{(k,i,j)}$, which shows the number of occurrences of error $e_m^{(k,i,j)}$ in calculating $Y_{i,j}^{(k)}$.

2) *Hessian*: We use the similar way as in [11] to calculate the Hessian of the loss L w.r.t. the error vector $e_m^{(k)}$. The Hessian matrix is of shape $2^{2N} \times 2^{2N}$ with each element calculated as follows:

$$\begin{aligned}
\frac{\partial^2 L}{\partial e_m^{(k)} \partial e_n^{(k)}} &= \frac{\partial}{\partial e_m^{(k)}} \left(\sum_{i=1}^N \frac{\partial L}{\partial z_i} \frac{\partial z_i}{\partial e_n^{(k)}} \right) \\
&= \sum_{i=1}^N \sum_{j=1}^N \frac{\partial z_i}{\partial e_m^{(k)}} \frac{\partial^2 L}{\partial z_i \partial z_j} \frac{\partial z_j}{\partial e_n^{(k)}} + \sum_{i=1}^N \frac{\partial L}{\partial z_i} \frac{\partial^2 z_i}{\partial e_m^{(k)} \partial e_n^{(k)}} \\
&\approx \sum_{i=1}^N \sum_{j=1}^N \frac{\partial z_i}{\partial e_m^{(k)}} \frac{\partial^2 L}{\partial z_i \partial z_j} \frac{\partial z_j}{\partial e_n^{(k)}} \quad (\text{assuming } \frac{\partial L}{\partial z_i} = 0),
\end{aligned}$$

where z_i is the i -th output of the model and $H_L(z)$ is the Hessian matrix of the loss L w.r.t. the output of the model z . Since our method starts with a pre-trained model that is converged, it can be assumed that $\frac{\partial L}{\partial z_i} = 0$ [11]. The whole Hessian matrix can thus be derived as:

$$H_{e^{(k)}} \approx J_z(e^{(k)})^T H_L(z) J_z(e^{(k)}), \tag{11}$$

where $J_z(e^{(k)})$ is the Jacobian matrix of the output vector z w.r.t. the error vector $e^{(k)}$. Note that we use the output of the model to expand the gradient because the final output vector has a smaller size than the vector of layer outputs. $J_z(e^{(k)})$ can be easily obtained by the same method used in deriving Eq. (10), where each element of it is calculated as follows:

$$\begin{aligned}
\frac{\partial z_k}{\partial e_m^{(k)}} &= \sum_{i=1}^N \sum_{j=1}^N \frac{\partial z_k}{\partial Y_{i,j}^{(k)}} \frac{\partial Y_{i,j}^{(k)}}{\partial e_m^{(k)}} \quad (\text{by chain rule}) \\
&= \sum_{i=1}^N \sum_{j=1}^N \frac{\partial z_k}{\partial Y_{i,j}^{(k)}} s_{ASW} c_m^{(k,i,j)} \quad (\text{by replacing } Y_{i,j}^{(k)} \text{ by Eq. (8)}),
\end{aligned}$$

where $\frac{\partial z_k}{\partial Y_{i,j}^{(k)}}$ is the gradient of k -th output of the model w.r.t. layer output $Y_{i,j}^{(k)}$, which can be easily obtained via back-propagation.

3) *Approximate Hessian*: Although the calculation of the Hessian matrix of the loss w.r.t. the error vector $e^{(k)}$ is far more efficient than GA and reinforcement learning-based algorithms, it takes hours to calculate the Hessian matrix on ImageNet. To improve the efficiency, we propose a fast way to approximate the Hessian matrix, providing a trade-off between accuracy and speed. The key idea is to approximate the Hessian matrix $H_L(z)$ by $v_{\max} \lambda_{\max} v_{\max}^T$, where λ_{\max} is the top eigenvalue and v_{\max} is the corresponding eigenvector. We apply power iteration method to calculate them efficiently. The Eq. (11) becomes:

$$\begin{aligned}
H_{e^{(k)}} &\approx J_z(e^{(k)})^T v_{\max} \lambda_{\max} v_{\max}^T J_z(e^{(k)}) \\
&= (J_z(e^{(k)})^T v_{\max}) \lambda_{\max} (J_z(e^{(k)})^T v_{\max})^T,
\end{aligned} \tag{12}$$

where $J_z(e^{(k)})^T v_{\max}$ is a Jacobian-vector product, which can be efficiently calculated with the built-in functions in PyTorch.

D. Optimized Selection of AppMuls

With the Taylor expansion estimation in Eq. (9), we propose to formulate the optimized selection of the AppMuls as an ILP problem. For the k -th layer, assume there are N_k different AppMuls for the bitwidth setting of that layer. We represent the choice of the AppMul by a one-hot vector $s^{(k)}$, where $s_i^{(k)} = 1$ ($1 \leq i \leq N_k$) represents that we select the i -th AppMul for the k -th layer. The perturbation of each candidate AppMul is calculated and stored in a vector $p^{(k)}$, where $p_i^{(k)}$ is the loss perturbation of applying the i -th candidate AppMul on the k -th layer, which is $\Omega^{(k, AM_k=i)}$ from Eq. (9). The formulation of the ILP algorithm is as follows:

$$\begin{aligned}
\min \quad & \sum_k (p^{(k)})^T s^{(k)}, \\
\text{subject to: } & \frac{\sum_k \text{Energy}^{(k, AM_k=s^{(k)})}}{\sum_k \text{Energy}^{(k, \text{Exact})}} \leq R_{\text{Energy}},
\end{aligned}$$

where $\text{Energy}^{(k, AM_k=s^{(k)})}$ is the total energy consumption of the k -th layer with the AppMul AM_k suggested by $s^{(k)}$ and R_{Energy} is an upper bound on the energy ratio between the approximate model and the exact model with given bitwidth setting for each layer.

Assume that the output tensor of the layer is of the shape $N_B \times N_O \times H \times W$, where N_B , N_O , H , and W are the batch size, number of the output channels, the height, and the width, respectively, and the weight tensor of the layer is of the shape $N_O \times N_I \times H_K \times W_K$, where N_I , H_K , and W_K are the number of the input channels, the kernel height, and the kernel width, respectively. We measure the energy consumption of all AppMuls used in this layer, denoted as $\text{Energy}^{(k, AM_k)}$ as follows:

$$\text{Energy}^{(k, AM_k)} = PDP_{AM_k} \cdot N_O \cdot H \cdot W \cdot N_I \cdot W_K \cdot H_K,$$

where PDP_{AM_k} is the power-delay product of the AppMul AM_k .

E. Calibration

After AppMul substitution on layers of the model, the layer outputs will change due to the errors introduced by the AppMuls. In order to eliminate the impact of these errors and recover the accuracy loss in a fast way, we apply a framework that can calibrate the input and weight tensor without the need of retraining, leveraging the LWC quantizer [19] discussed in Section III-D.

The detailed procedure is shown in Algorithm 1. For each layer k , we first optimize the scaling factor $s_{X^{(k)}}^*$ for quantizing $X^{(k, AM_k)}$ to minimize the mean relative error (MRE) between the original input matrix $X^{(k)}$ and the input matrix $X^{(k, AM_k)}$ after approximation. Then, we apply the LWC quantizer to optimize the lower bound $\gamma^{(k)}$ and the upper bound $\beta^{(k)}$ for the weight matrix $W^{(k)}$ as illustrated in Section III-D.

Fig. 2 shows the distributions of the difference between the outputs produced by the exact and the approximate multipliers, with one distribution before the calibration and the other after calibration. After calibration, the distribution of the outputs produced by the AppMuls at each layer is much closer to that produced by the exact multipliers. Therefore, the calibration process can effectively reduce the approximation error, enabling the model to recover from most of the accuracy loss.

V. EVALUATION RESULTS

A. Experimental Setup

FAMES is built on CUDA v12.1 and PyTorch v2.3.1. All experiments are conducted on an Nvidia RTX 4090 24GB GPU with an Intel Xeon Platinum 8338C CPU. We validate our framework on several

Algorithm 1 The calibration procedure

Require: Sample dataset S , approximate model M , number of epochs N_{epochs} , learning rate lr

Ensure: Optimal scaling factor $s_{X^{(k)}}^*$, upper bound $\gamma^{(k)}$, and lower bound $\beta^{(k)}$ for each layer k

for all input matrix $X^{(k, AM_k)}$ in M **do**

for $q \in [0, 0.5)$ with step = 0.01 **do**

$X_q^{(k, AM_k)} \leftarrow \text{quantile}(X^{(k, AM_k)}, q, 1 - q)$

end for

$q^* \leftarrow \arg \min_q \text{MRE}(X_q^{(k, AM_k)}, X^{(k)})$

$s_{X^{(k)}}^*$ is the scaling factor of $X_q^{(k, AM_k)}$

end for

for $i = 1$ to N_{epochs} **do**

for all batch in S **do**

Calculate $\frac{\partial L}{\partial \gamma^{(k)}}$ and $\frac{\partial L}{\partial \beta^{(k)}}$ based on Section III-D

$\gamma^{(k)} \leftarrow \gamma^{(k)} - lr \cdot \frac{\partial L}{\partial \gamma^{(k)}}$

$\beta^{(k)} \leftarrow \beta^{(k)} - lr \cdot \frac{\partial L}{\partial \beta^{(k)}}$

end for

end for

return $s_{X^{(k)}}^*$, $\gamma^{(k)}$, and $\beta^{(k)}$ for each layer k

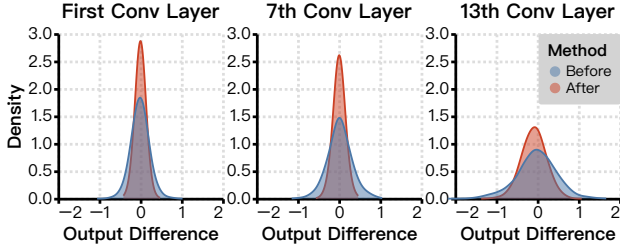


Fig. 2. Distribution of the difference between the outputs using exact multipliers and using AppMuls in ResNet-20. Two cases are compared before and after calibration for the approximate output.

models, including the ResNet family, VGG-19, and SqueezeNet. We use AppMuls from EvoLib8b [18] for comparison with approximation works which use $8 \times N$ -bit models and we apply ALSRAC [20] to generate low-bitwidth AppMuls for comparison with quantization works. ALSRAC supports various error metrics. Among them, we choose the mean relative error distance (MRED) as the metric and set the threshold to 20%. The delays and powers of the AppMuls are based on the simulation result of Synopsys Design Compiler [21] with the NanGate 45nm open cell library [22]. We take the exact multipliers from the library as the multipliers used in the quantization-only work. Unless otherwise specified, the batch size of samples for perturbation estimation is 256 and all accuracy results are obtained with a sample dataset of size 1024 through 5 epochs of calibration and a learning rate $lr = 0.1$.

B. Performance of the Proposed AppMul Selection Method

This section studies the performance of our proposed ILP-based AppMul selection method. We compare it with two existing works, ALWANN [8] and MARLIN [9], which also propose method for choosing the optimized AppMuls.

In Fig. 3, we tested the approximate models obtained by our method under the same energy constraints for ResNet-8, ResNet-14, and ResNet-50 on CIFAR-10. Our approximate models can reduce the energy consumption with minor accuracy loss, or achieve much better accuracy with similar energy consumption compared to MARLIN [9] and ALWANN [8]. This shows the effectiveness of our proposed AppMul selection method. In Table II, the runtime for selecting the optimized AppMuls in each method and the runtime of the other

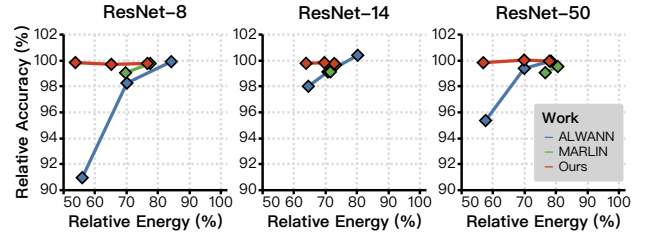


Fig. 3. Relative accuracy vs. relative energy for approximate models obtained with different multiplier selection methods. Relative values are calculated with respect to the performance of the exact 8-bit quantized model on CIFAR-10 in each corresponding paper.

TABLE II
RUNTIME OF MULTIPLIER SELECTION METHODS.

	This Work		MARLIN [9]		ALWANN [8]	
	Select Time	Other Time ¹	Select Time	Other Time ¹	Select Time	Other Time ¹
ResNet-8	0.02 h	0.004 h	10.6 h	0.41 h	10.4 h	6.2 h
ResNet-14	0.06 h	0.006 h	12.0 h	0.60 h	41.7 h	12.1 h
ResNet-50	0.27 h	0.02 h	109.9 h	1.15 h	134.2 h	45.4 h

¹ Other time is the runtime besides AppMul selection, which is the calibration time for our work, training time for MARLIN [9], and validation time for ALWANN [8].

components required to recover the model accuracy in each method are compared. Since our method does not require as many iterations as NSGA-II used in other works to find the optimal approximate configurations, and requires little time to recover accuracy through calibration, it took much less time in both situations compared to the other works. This shows the efficiency of our proposed method.

C. Model Performance Comparison

Table III compares our results with other quantization works with different bitwidth configurations and approximation works that use uniform multipliers across the model. It shows the recovered accuracy, the relative accuracy, and the relative energy with respect to the baseline 8-bit quantized exact model.

Compared with the approximation works [13] and AdaPT [14], our method saves 15.24% to 23.90% of the energy with much better accuracy results, using multipliers of the same bitwidth settings. In addition, both of these approximation works only support $8 \times N$ multiplications, while our work is able to significantly improve the efficiency of the model again at much lower bits. Compared with the mixed-precision quantization works such as HAWQ [23] and HAWQ-V3 [7], our method combined with the 8×8 or 4×4 mixed-precision configuration can further reduce the energy consumption by 33.31% to 35.11% with slight improvement in accuracy. When combined with 2/3-bit uniform quantization, our model can minimize the energy consumption of the model while still maintaining high accuracy. The obtained approximate models reduce 20.41% to 35.90% of the energy consumption with a maximum accuracy degradation of 0.44%, or even better accuracy compared to PACT [12] and the baseline 2/3-bit exact models.

On average, by AppMul substitution with our method, we achieve a 28.67% energy reduction over corresponding quantized models of the same bitwidth with accuracy degradation less than 1%.

VI. ABLATION STUDY

This section performs the ablation study for FAMES, focusing on three essential parts in FAMES: the perturbation estimation, the selection algorithm, and the calibration method.

TABLE III
THE ACCURACY AND ENERGY RESULTS OF RELATED WORK AND THE PROPOSED WORK.

Model	Work	Bit-Width ¹		Multiplier	Accuracy (%)	Relative ² Accuracy (%)	Relative ² Energy (%)	Reduced ³ Energy (%)
ResNet-20 (CIFAR-10)	Baseline	8	8	Accurate	92.49	100.00	100.00	-
	[13]	8	8	Approximate	88.17	95.33	88.00	-
		4	8	Approximate	86.94	94.00	31.30	-
	Ours	8	8	Mixed ⁴	92.59	100.11	66.97	23.90
		4	8	Mixed ⁴	92.05	99.52	24.96	20.26
	HAWQ [23]	4.11	4.21	Accurate	92.22	99.71	8.26	-
	Ours	4.11	4.21	Mixed ⁴	92.30	99.79	5.36	35.11
	PACT [12]	3	3	Accurate	91.10	98.50	2.11	-
		2	2	Accurate	89.70	96.98	1.17	-
	Ours	3	3	Mixed ⁴	91.13	98.53	1.45	31.28
		2	2	Mixed ⁴	89.26	96.51	0.75	35.90
VGG-19 (CIFAR-10)	Baseline	8	8	Accurate	94.09	100.00	100.00	-
	AdaPT [14]	8	8	Approximate	93.56	99.44	73.21 ⁵	-
	Ours	8	8	Mixed ⁴	93.77	99.66	62.05	15.24
	Baseline	3	3	Accurate	91.83	97.60	1.47	-
	Ours	3	3	Mixed ⁴	92.19	97.98	1.17	20.41
SqueezeNet (CIFAR-100)	Baseline	8	8	Accurate	71.59	100.00	100.00	-
	Baseline	3	3	Accurate	71.34	99.65	7.63	-
		2	2	Accurate	69.04	96.44	6.74	-
	Ours	3	3	Mixed ⁴	71.95	100.50	5.08	33.42
		2	2	Mixed ⁴	68.92	96.27	4.61	31.60
ResNet-18 (ImageNet)	Baseline	8	8	Accurate	71.47	100.00	100.00	-
	HAWQ-V3 [7]	6.12	6.12	Accurate	70.38	98.48	54.54	-
		5.17	5.17	Accurate	69.72	97.56	33.32	-
	Ours	6.12	6.12	Mixed ⁴	70.94	99.26	36.37	33.31
		5.17	5.17	Mixed ⁴	70.72	98.96	21.67	34.96

- ¹ Refer to the average bitwidth across layers for mixed-precision models.
² Calculated w.r.t. the baseline models, which use exact 8×8 multipliers.
³ Compared with the related work that has the same bit-width setting.
⁴ Use mixed AppMuls across layers.
⁵ Implemented in NanGate 45nm open cell library [22].

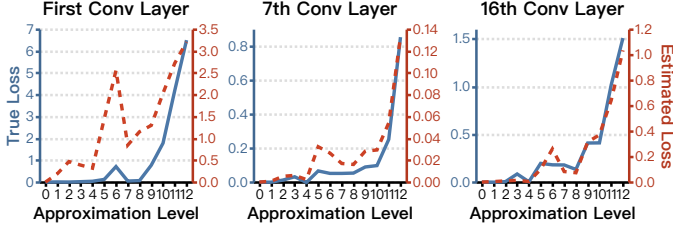


Fig. 4. True loss vs. Taylor expansion estimation for ResNet-20 with 4×4 AppMuls at different approximation levels.

A. Effect of Perturbation Estimation

We demonstrate the effect of our method for estimating the loss perturbation by applying AppMuls to each layer. The experiment is conducted on Resnet-20 with CIFAR-10 data using uniform 4-bit quantization. For each layer, we apply every AppMuls generated by ALSRAC [20] and estimate their loss perturbation respectively, which are then compared with the true loss perturbation by directly testing on the dataset. The result is shown in Fig. 4. The difference of value is due to the change of the gradient value in the exact model after approximation. Despite that, our estimation is consistent with the actual trend of the loss.

B. Effect of the AppMul Selection Algorithm

Our AppMul selection algorithm is based on the perturbation estimation and the ILP algorithm. We validate its advantage in both

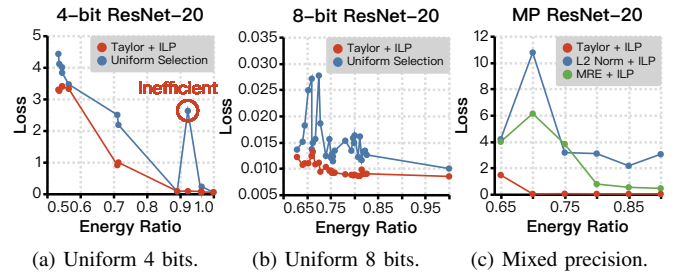


Fig. 5. Comparison of our method with other methods in uniform bitwidth and mixed bitwidth.

uniform and mixed-precision bitwidth settings. All the following experiments are conducted on ResNet-20 in CIFAR-10 dataset. First, we apply a uniform 4-bit or 8-bit setting, respectively. Fig. 5(a) and Fig. 5(b) compare the loss perturbation by our selection algorithm and by uniform selection. It can be seen that our method achieves a lower loss than the uniform selection with the same energy ratio constraint. It is because there are some inefficient multipliers in the library that result in a large loss perturbation, as circled out in Fig. 5(a), and our method manages to avoid them. Then, we apply the mixed-precision setting in the paper [7]. In this case, we cannot perform uniform selection, so we compare our Taylor expansion-based perturbation estimation with other estimators, including the L2 norm of error matrix and MRE of the AppMul. As shown in Fig. 5(c), our method

TABLE IV
RECOVERED ACCURACY AND RUNTIME WITH DIFFERENT METHODS.

Model	BitWidth		Retraining Method		Calibration Method	
	W	A	Acc (%)	Time (s)	Acc (%)	Time (s)
ResNet-20 (CIFAR-10)	8	8	92.49		92.59	
	4	8	91.83		92.05	
	4.1	4.2	90.50	74.6	92.3	13.2
	3	3	91.63		91.13	
VGG-19 (CIFAR-10)	2	2	89.34		89.26	
	8	8	93.79		93.77	
SqueezeNet (CIFAR-100)	3	3	71.48		71.95	
	2	2	68.86	73.5	68.92	8.6
ResNet-18 (ImageNet)	6.1	6.1	69.32		70.94	
	5.2	5.2	68.38	4659.9	70.72	79.3

outperforms the others, since it can recognize the importance of each layer and assign relatively exact multipliers to layers with a strong impact on the model. In conclusion, our method outperforms the uniform selection in uniform bitwidth settings and is especially helpful for the mixed-precision bitwidth setting.

C. Effect of the Calibration Method

Table IV shows the impact of the calibration method. It compares the accuracy and the runtime recovered by retraining, and by calibration. The retraining results are generated after performing retraining for 5 epochs. It can be seen that, with the calibration method, approximate models can be restored to a similar accuracy as retraining in a much shorter time. In some cases, even better accuracy can be achieved by calibration than short-epoch retraining, proving that the calibration method can efficiently reduce the errors introduced by AppMuls.

VII. CONCLUSIONS

The marriage between the general approximate multipliers and the extremely low-bitwidth quantization is achieved for modern DNN models! This is enabled by our systematic solution, FAMES, which efficiently selects the optimal AppMul configuration with different bitwidth settings, and restores the accuracy of the approximate model without retraining. To the best of our knowledge, this is the first AppMul substitution work to support multiplications with bitwidth down to 2 bits. It achieves an average of 28.67% energy reduction over the corresponding quantized model of the same bitwidth with a small accuracy degradation within 1%. In the future, we will extend FAMES to other AI models, including large language models.

REFERENCES

- [1] B. Alshemali and J. Kalita, "Improving the reliability of deep neural networks in nlp: A review," *Knowledge-Based Systems*, vol. 191, p. 105210, 2020.
- [2] W. Yin, K. Kann, M. Yu, and H. Schütze, "Comparative study of cnn and rnn for natural language processing," 2017. [Online]. Available: <https://arxiv.org/abs/1702.01923>
- [3] Z. Peng, S. Li, G. Chen, C. Zhang, H. Zhu, and M. Xue, "Fingerprinting deep neural networks globally via universal adversarial perturbations," in *2022 IEEE/CVF Conference on Computer Vision and Pattern Recognition (CVPR)*, 2022, pp. 13 420–13 429.
- [4] J. Hu, L. Cao, T. Tong, Q. Ye, S. Zhang, K. Li, F. Huang, L. Shao, and R. Ji, "Architecture disentanglement for deep neural networks," in *2021 IEEE/CVF International Conference on Computer Vision (ICCV)*, 2021, pp. 652–661.

- [5] S. Kundu, S. Wang, Q. Sun, P. A. Beerel, and M. Pedram, "Bmpq: Bit-gradient sensitivity-driven mixed-precision quantization of dnns from scratch," in *2022 Design, Automation & Test in Europe Conference & Exhibition (DATE)*, 2022, pp. 588–591.
- [6] K. Wang, Z. Liu, Y. Lin, J. Lin, and S. Han, "Hq: Hardware-aware automated quantization with mixed precision," 2019. [Online]. Available: <https://arxiv.org/abs/1811.08886>
- [7] Z. Yao, Z. Dong, Z. Zheng, A. Gholami, J. Yu, E. Tan, L. Wang, Q. Huang, Y. Wang, M. Mahoney *et al.*, "Hawq-v3: Dyadic neural network quantization," in *International Conference on Machine Learning*. PMLR, 2021, pp. 11 875–11 886.
- [8] V. Mrazek, Z. Vasíček, L. Sekanina, M. A. Hanif, and M. Shafique, "Alwann: Automatic layer-wise approximation of deep neural network accelerators without retraining," in *2019 IEEE/ACM International Conference on Computer-Aided Design (ICCAD)*. IEEE, 2019, pp. 1–8.
- [9] F. Guella, E. Valpreda, M. Caon, G. Masera, and M. Martina, "Martlin: A co-design methodology for approximate reconfigurable inference of neural networks at the edge," *IEEE Transactions on Circuits and Systems I: Regular Papers*, 2024.
- [10] A. Gholami, S. Kim, Z. Dong, Z. Yao, M. W. Mahoney, and K. Keutzer, "A survey of quantization methods for efficient neural network inference," in *Low-Power Computer Vision*. Chapman and Hall/CRC, 2022, pp. 291–326.
- [11] Y. Li, R. Gong, X. Tan, Y. Yang, P. Hu, Q. Zhang, F. Yu, W. Wang, and S. Gu, "Brecq: Pushing the limit of post-training quantization by block reconstruction," *arXiv preprint arXiv:2102.05426*, 2021.
- [12] J. Choi, Z. Wang, S. Venkataramani, P. I.-J. Chuang, V. Srinivasan, and K. Gopalakrishnan, "Pact: Parameterized clipping activation for quantized neural networks," *arXiv preprint arXiv:1805.06085*, 2018.
- [13] V. Mrazek, L. Sekanina, and Z. Vasíček, "Libraries of approximate circuits: Automated design and application in CNN accelerators," *IEEE Journal on Emerging and Selected Topics in Circuits and Systems*, vol. 10, no. 4, pp. 406–418, 2020.
- [14] D. Danopoulos, G. Zervakis, K. Siozios, D. Soudris, and J. Henkel, "Adapt: Fast emulation of approximate dnn accelerators in pytorch," *IEEE Transactions on Computer-Aided Design of Integrated Circuits and Systems*, vol. 42, no. 6, pp. 2074–2078, 2022.
- [15] T. Yu, B. Wu, K. Chen, C. Yan, and W. Liu, "Toward efficient retraining: A large-scale approximate neural network framework with cross-layer optimization," *IEEE Transactions on Very Large Scale Integration (VLSI) Systems*, 2024.
- [16] D. Zhang, J. Yang, D. Ye, and G. Hua, "Lq-nets: Learned quantization for highly accurate and compact deep neural networks," in *Proceedings of the European conference on computer vision (ECCV)*, 2018, pp. 365–382.
- [17] K. Deb, A. Pratap, S. Agarwal, and T. Meyarivan, "A fast and elitist multiobjective genetic algorithm: Nsga-ii," *IEEE Transactions on Evolutionary Computation*, vol. 6, no. 2, pp. 182–197, 2002.
- [18] V. Mrazek, R. Hrbacek, Z. Vasíček, and L. Sekanina, "Evoapprox8b: Library of approximate adders and multipliers for circuit design and benchmarking of approximation methods," in *Design, Automation & Test in Europe Conference & Exhibition (DATE)*, 2017, 2017, pp. 258–261.
- [19] W. Shao, M. Chen, Z. Zhang, P. Xu, L. Zhao, Z. Li, K. Zhang, P. Gao, Y. Qiao, and P. Luo, "Omniquant: Omnidirectionally calibrated quantization for large language models," *arXiv preprint arXiv:2308.13137*, 2023.
- [20] C. Meng, W. Qian, and A. Mishchenko, "Alsrac: Approximate logic synthesis by resubstitution with approximate care set," in *2020 57th ACM/IEEE Design Automation Conference (DAC)*, 2020, pp. 1–6.
- [21] Synopsys Inc., <http://www.synopsys.com>, 2021.
- [22] Nangate, Inc., "Nangate 45nm open cell library," <https://si2.org/open-cell-library/>, 2022.
- [23] Z. Dong, Z. Yao, A. Gholami, M. W. Mahoney, and K. Keutzer, "Hawq: Hessian aware quantization of neural networks with mixed-precision," in *Proceedings of the IEEE/CVF international conference on computer vision*, 2019, pp. 293–302.